Volume 16
Number 2

December *2014*
(ISSN 1109-1606)

Journal of APPLIED ELECTROMAGNETISM

JAE

Institute of Communication and Computer Systems

Athens - GREECE

Volume 16 December 2014
Number 2 (ISSN 1109-1606)

JOURNAL
OF
APPLIED ELECTROMAGNETISM

Institute of Communication and Computer Systems

Athens - GREECE

Volume 16 **Number 2**

December 2014

TRANS BLACK SEA REGION UNION OF APPLIED ELECTROMAGNETISM (BSUAE)

JOURNAL OF APPLIED ELECTROMAGNETISM

Institute of Communication and Computer Systems

Athens - GREECE

Editor: Panayiotis Frangos (Greece), pfrangos@central.ntua.gr

Honorary Editor: Nikolaos K. Uzunoglu (Greece), nuzu@central.ntua.gr

Board of Associate Editors

D. Dimitrov (Bulgaria), dcd@tu-sofia.bg
V. Dumbrava (Lithuania), vydum@ktu.lt
G. Georgiev (Bulgaria), gngeorgiev@yahoo.com
G. Matsopoulos (Greece), gmatso@esd.ece.ntua.gr

Editorial Board

ALBANIA
G. Bardhyf, bardhylgolemi@live.com
C. Pirro, p_cipo@yahoo.com

ARMENIA
H. Bagdasarian, hovik@seua.sci.am
H. Terzian, hterzian@seua.sci.am

BULGARIA
A. Antonov, asantonov@abv.bg
A. Lazarov, lazarov@bfu.bg
S. Savov, savovsv@yahoo.com

GEORGIA
R. Zaridze, rzaridze@laetsu.org

GERMANY
M. Georgieva – Grosse, mngeorgieva@yahoo.de

GREECE
H. Anastassiu, ANASTASIOU.Christos@haicorp.com
I. Avramopoulos, hav@mail.ntua.gr
G. Fikioris, gfiki@cc.ece.ntua.gr
J. Kanellopoulos, ikanell@cc.ece.ntua.gr
G. Karagiannidis, geokarag@auth.gr
G. Kliros, gsksma@hol.gr
T. Mathiopoulos, mathio@space.noa.gr
C. Moschovitis, harism@noc.ntua.gr
K. Nikita, knikita@cc.ece.ntua.gr
I. Ouranos, iouranos@central.ntua.gr
E. Papkelis, spapkel@central.ntua.gr
J. Sahalos, sahalos@auth.gr
M. Theologou, theolog@cs.ntua.gr

N. Triantafyllou, nitriant@central.ntua.gr
K. Ksystra, katksy@central.ntua.gr
A. Malamou, annamalamou@yahoo.gr

JORDAN
N. Dib, nihad@just.edu.jo

KAZAKSHTAN
S. Sautbekov, sautbek@mail.ru

LITHUANIA
L. Svilainis, linas.svilainis@ktu.lt

RUSSIA
M. Bakunov, bakunov@rf.unn.runnet.ru
A. Grigoriev, adgrigoriev@mail.ru

SERBIA
B. Reljin, ereljin@ubbg.etf.bg.ac.yu

SPAIN
E. Gago – Ribas, egr@tsc.uniovi.es
M. Gonzalez – Morales, gonmor@yllera.tel.uva.es

UNITED KINGDOM
G. Goussetis, G.Goussetis@hw.ac.uk

Publishing Department

M. Georgieva – Grosse, mngeorgieva @yahoo.de
N. Triantafyllou, nitriant@central.ntua.gr
K. Ksystra, katksy@central.ntua.gr
A. Malamou, annamalamou@yahoo.gr

Journal of Applied Electromagnetism

Copyright Form

The undersigned I confirm that I agree the publication of the article

in the Journal of Applied Electromagnetism and the copyright to belong to Trans Black Sea Union of Applied Electromagnetism. I understand that I have the full right to reuse this manuscript for my own purposes.

Name:

Surname:

Address:

E-mail:

Signed:

***Please send the previous form signed either by e-mail to pfrangos@central.ntua.gr , or by fax to the fax number: +30 210 772 2281, attention of Prof. P. Frangos.**

Address

Institute of Communication and Computer Systems

National Technical University of Athens

9, Iroon Polytechniou str.

15773 Athens - GREECE

Tel: (+30) 2107723694

Fax: (+30) 2107722281, attention of Prof. P. Frangos

e-mail: pfrangos@central.ntua.gr

Web site: **http://jae.ece.ntua.gr**

TRANS BLACK SEA REGION UNION OF APPLIED ELECTROMAGNETISM (BSUAE)

JOURNAL OF APPLIED ELECTROMAGNETISM (JAE)

Volume 16 Number 2 December 2014

CONTENTS

THE MAGNETIZATION CONDITIONS OF MODELING OF THE ACTION OF MAGNETIC PARTICLES IN MAGNETIC FLUIDS

K.V. Kotetishvili and G.G. Chikhladze 1

In MRI three kinds of magnetic flux density are applied: the first – strong B0 field in z-direction, the second – B1 transverse radio-frequency wave and the third – space-coded fields (G gradients) in z-directions as well. In the paper low (sick) fields of 0.1 Tl – 0.35 Tl are considered. In such kind of low fields the fluid is unable to reach saturation and nano-particles revolve in additional rotating magnetic field. The magnetization in magnetic fluids increases in spiral form.

EXPERIMENTAL INVESTIGATION ON SPACE CONFIGURATION AND INFLUENCE OF ELECTROMAGNETIC FIELD OF SHORT WAVE APPARATUSES IN MEDICAL THERAPY

D. Dimitrov and A.P. Petrova 7

The usage of short waves in the medical therapy started to become quite popular in the recent decades. The space-time configuration research of the electromagnetic field in the patient area within the UHF range is really important for the treatment used in physiotherapy methods. Based on the results of this study are defined the system's mode which induce the electromagnetic field in the patient area, the number of the therapeutic procedures and duration of each of them. The radiators (antennas) in the physiotherapy are often in proximity to the patient's body, i.e it is necessary to consider the impact of the body to the patient, the parameters of the antenna and to the research of the area in the near field. In this paper are presented and described in graphic form the conducted studies for electromagnetic field strength in the very near field in real clinical conditions.

At high frequencies, polarizing molecules are in the patient's body completely failed changing their spatial orientation and appear vibrations of the dipoles around neutral position. This process is related to the generation of heat. A characteristic feature of UHF waves impact on the body that the heat is produced within the body itself. In physiotherapy are used transmitters, which excited the electrical field for the induction of these frequencies. A pair of two "electrodes" usually acts as antenna system on these devices. The antenna system is ensuring the influence of the electromagnetic field of a small part of the human body.

MEASUREMENT AND COMPARISON OF LTE AND HSPA+ NETWORK PARAMETERS

D. Rukavičius, V. Grimaila and S. Kašėta **15**

Long Term Evolution (LTE) network parameters are analysed in this paper. 3GPP LTE Release 8 specifies peak downlink throughput up to 100 Mbps using SISO antennas and up to 300 Mbps using 4x4 MIMO antennas. According Channel Quality Indicator (CQI) and Received Signal Strength Indicator (RSSI) indexes the Physical Downlink Shared Channel (PDSCH) download throughput of LTE network there is analysed in dependency of distance from base stations. Throughput values are compared with the results of High Speed Packet Access (HSPA+) network measurements as this is earlier technology for data transfer. HSPA+ and LTE networks measurements were made in implemented real network in real time. As LTE network on measuring time was not used by other users yet, the results of analysis can be considered as received in real and close to ideal conditions. HSPA+ network was used by users, but values are close to ideal as the network was newly implemented.

RF EXPOSURE SIMULATION USING BLOOD PERFUSION FOR A CHILD AND WOMAN MODELS

V. Jeladze, M. Prishvin and R. Zaridze **26**

It is known, that conventional Pennes bio-heat equation does not consider blood perfusion. The motivation of this paper is to conduct a comparative analysis of the temperature and temperature rise during EM exposure, obtained using conventional pennes bio-heat equation and a modified model considering blood perfusion. The non-homogeneous discreet models of a child and a woman were used for simulation.

THE MAGNETIZATION CONDITIONS OF MODELING OF THE ACTION OF MAGNETIC PARTICLES IN MAGNETIC FLUIDS

K.V. Kotetishvili and G.G. Chikhladze

Georgian Technical University,
0175, 77, M. Kostava str., Tbilisi, Georgia,
ketinooo@hotmail.com

Abstract

In MRI three kinds of magnetic flux density are applied: the first – strong B_0 field in z-direction, the second – B_1 transverse radio-frequency wave and the third – space-coded fields (G gradients) in z-directions as well. In the paper low (sick) fields of 0.1 Tl – 0.35 Tl are considered. In such kind of low fields the fluid is unable to reach saturation and nano-particles revolve in additional rotating magnetic field. The magnetization in magnetic fluids increases in spiral form.

1. INTRODUCTION

In MRI three kinds of magnetic flux density are applied: the first – strong B_0 field in z-direction, the second – B_1 transverse radio-frequency wave and the third – space-coded fields (G gradients) in z-directions as well.

B_0 field of about 1.5 Tl is induced by polarization of nuclear spins. Then relatively less will be B_1 field (approximately 0.01 Tl), used for transportation of induced magnetization into transverse component of the pattern as well, as G gradients (~10 mTl/m), used for the space coding of the transfer magnetization.

For high B_0 fields at ordinary MRI it shows that the equilibrium of the magnetization for magnetic fluids will be saturated and the particles of the fluid will be in accordance with B_0, i.e. will be lined in B_0 direction [1, 2].

In the paper low (sick) fields of 0.1 Tl – 0.35 Tl are considered. In such kind of low fields the fluid is unable to reach saturation (is not completed) and nano-particles revolve in additional, also revolving magnetic field.

2. MAGNETIZATION IN LOW/SICK FIELDS - BASIC EQUATIONS

Under an action of a magnetic field the expression for relaxation of the magnetization for magnetic fluids is given as follows

$$\frac{\partial \vec{M}}{\partial t} + \vec{\upsilon} \cdot \nabla \vec{M} - \vec{\omega} \times \vec{M} + \left(\frac{1}{\tau}\right)\left(\vec{M} - \vec{M}_{sat}\right) = 0, \quad (1)$$

which at the same time provides as the magnetization, as the re-orientation of given field. $\vec{\upsilon}$ is the vector of linear velocity of the magnetic fluid, while $\vec{\omega}$ the vector of spin velocity of the magnetic fluid and $\tau -$ its time of relaxation.

The left-hand-side of (1) is straightly dependent on $\vec{\upsilon}$ velocity of the linear motion and on $\vec{\omega}$ angular (spin) velocity. The equation of state in the magnetic field possesses the time constant characteristic for the equilibrium magnetization, described by the following expression:

$$\frac{1}{\tau} = \frac{1}{\tau_B} + \frac{1}{\tau_N}, \quad (2)$$

τ_B, τ_N being Brown's and Neel's times of relaxation, respectively, given as follows:

$$\tau_B = \frac{3V_h\mu_C}{kT}, \quad (3)$$

$$\tau_N = \tau_0 \cdot e^{\frac{k_\alpha V_p}{kT}}, \quad (4)$$

V_h being the hydrodynamic volume of nano-particles in m^3, while $\mu_C -$ the dynamic viscosity of the given fluid (ns/m^2), k – Boltzmann's constant, T – the absolute temperature (if no other hints are given, assume 295 K or 22 ^{0}C). V_p is the volume of nano-particles in m^3 (excluding the active external particles), k_α being the anisotropic constant (J/m^3) and τ_0 is Neel's time characteristic (in nano-seconds). Usually $\tau \approx 10^{-9} \div 10^{-10}$ s. In (2) the smallest time constant is denoted by τ. Thus, at Brown's and Neel's relaxation the radius of particles increases.

Neel's relaxation, describing the rotation of the magnetization vector of particles, usually dominates for small particles of less, than 4 nm radius, while Brown's relaxation, due to rotation of the particles in a fluid, dominates for the particles of radius, exceeding 4 nm.

If the number of particles in a magnetic fluid is fixed (for example, being located at its surface), the only Neel's relaxation is in action, while Brown's relaxation is absent.

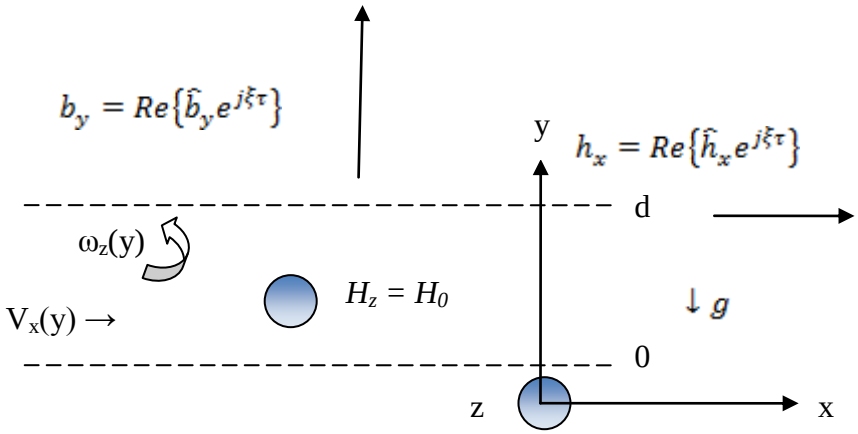

Figure 1.

In figure 1 the flux of a magnetic fluid is presented in the fixed area (y = 0, y = d) The trended flux is pumped by H_0 magnetic field acting in z direction and by x directed sinusoidal magnetic field of the sick signal with the complex amplitude $\hat{h}_x$ as well, as in y direction by the sinusoidal magnetic fluctuation density of the sick signal with the complex amplitude $\hat{b}_y$. In x and y directions the components of the magnetic field vary due to the sinusoidal law with ξ frequency. $v_x(y)$ velocity is directed along x-axis, while the spin velocity $\omega_z(y)$ – along z-axis and both are y dependent.

As it is seen in figure, the velocity of the flux bleeding is directed only along x-axis while time-average spin velocity – only along z-direction. Both are space distinguished in y-dependence:

$$\vec{v} = v_x(y)\vec{i}_x, \tag{5}$$

$$\vec{\omega} = \omega_z(y)\vec{i}_z. \tag{6}$$

Taking into account the distribution of magnetic field strengths (densities) as they are given in figure, $\vec{i}_x$ and , $\vec{i}_z$ are space homogeneous due to corresponding zero space derivatives. Due to Ampere's law, given in the form of

$$\vec{\nabla} \times \vec{H} = \vec{j} + \frac{\partial \vec{D}}{\partial t} = 0, \tag{7}$$

when the conductivity is zero $(\vec{j} = 0)$ or the change in current density differs from it $\left(\partial\vec{D}/_{\partial t} \neq 0\right)$, the field strength should be zero and given by (7) surely.

As it is seen in figure, both x and z components of the intensity of the magnetic field are homogeneous, when H_0 is invariant in space. It is seen as well that the field derivatives due to x and z are taken as zero, while the pressure gradient $\partial\rho/\partial x$ may differ from zero, being additionally independent on the linear flux (at its absence as well). As it follows from (7)

$$\frac{\partial(H_0)}{\partial y} - \frac{\partial h_y}{\partial z} = 0. \tag{8}$$

From (8) yields thus

$$\frac{\partial(H_0)}{\partial y} = 0, \quad \text{and} \quad \frac{\partial h_y}{\partial z} = 0 \tag{9}$$

as well, as

$$\frac{\partial h_x}{\partial z} - \frac{\partial(H_0)}{\partial x} = 0 \tag{10}$$

and

$$\frac{\partial h_x}{\partial z} = 0 \quad \text{and} \quad \frac{\partial(H_0)}{\partial x} = 0 \tag{11}$$

and

$$\frac{\partial h_y}{\partial x} - \frac{\partial h_x}{\partial y} = 0. \tag{12}$$

From (12) follows

$$\frac{\partial h_y}{\partial x} = 0 \quad \text{and} \quad \frac{\partial h_x}{\partial y} = 0. \tag{13}$$

Gauss's law regulates densities of the fixed magnetic flux along i_y :

$$\vec{\nabla}\cdot\vec{B} = \frac{\partial b_x}{\partial x} + \frac{\partial b_y}{\partial y} + \frac{\partial(B_0)}{\partial z} = 0. \tag{14}$$

Then we get

$$\frac{\partial b_y}{\partial y} = 0, \tag{15}$$

when

$$\frac{\partial b_x}{\partial x} = \frac{\partial(B_0)}{\partial z} = 0. \tag{16}$$

Based on this survey we may conclude that b_y and h_x should be constant in space and independent on y, while h_y may be dependent on y, when y itself depends on m_y.

The density of total instantaneous magnetic fluctuations $\vec{B}$, total instantaneous magnetic field $\vec{H}$ and total instantaneous magnetization $\vec{M}$ are given as follows

$$\vec{B} = Re\{(\hat{b}_x(y)\vec{i}_x + \hat{b}_y\vec{i}_y)e^{j\xi t}\} + B_0\vec{i}_z, \tag{17}$$

$$\vec{H} = Re\{(\hat{h}_x\vec{i}_x + \hat{h}_y(y)\vec{i}_y)e^{j\xi t}\} + H_0\vec{i}_z, \tag{18}$$

$$\vec{M} = Re\{(\hat{m}_x(y)\vec{i}_x + \hat{m}_y(y)\vec{i}_y)e^{j\xi t}\} + M_0\vec{i}_z, \tag{19}$$

while the relation between $\vec{B}$, $\vec{H}$ and $\vec{M}$ is given in the following way:

$$\vec{B} = \mu_0(\vec{H} + \vec{M}), \tag{20}$$

h_x and h_y are functions varying in time due to the sinusoidal law, while $h_z = 0$. Here application of the total amplitude of rotation is acceptable. " $\hat{}$ " represents the complex amplitude, while Re – shows the real part of a complex quantity. ξ is the frequency in rad/s and $j = \sqrt{-1}$.

Relation between M_0 and M_{equil} is given by [3]

$$M_0 = M_{equil}L(\alpha_0), \tag{21}$$

$L(\alpha_0)$ showing the sequence of magnetic nano-particles for given magnetic field of $|H|$ magnitude. Here is the sick signal of the magnetic field, which itself represents the absence of dependence of the sick signal along i_z. Thus, z component of the magnetization is the dipole signal and is given by the equilibrium quantity of M_0. For solution of the instantaneous magnetization fixed $\hat{b}_y$ and $\hat{h}_x$ fields take the shape of the source of the signal.

According to these circumstances for the expression (1) x and y (transversal) components will be given by the following formulae:

$$j\xi\hat{m}_x + \omega_z\hat{m}_y + \frac{1}{\tau}\left(\hat{m}_x - \frac{M_0}{H_0}h_x\right) = 0 \tag{22}$$

and

$$j\xi\hat{m}_y - \omega_z\hat{m}_x + \frac{1}{\tau}\left(\hat{m}_y - \frac{M_0}{H_0}h_y\right) = 0, \tag{23}$$

where $\hat{m}_x$ and $\hat{m}_y$ are functions of the spin velocity ω_z and are given by the following expressions:

$$\hat{m}_x = \frac{M_0}{H_0}\cdot\frac{\left(j\xi\tau + 1 + \frac{M_0}{H_0}\right)\hat{h}_y - (\omega_z\tau)\frac{\hat{b}_y}{\mu_0}}{(j\xi\tau + 1)\left(j\xi\tau + 1 + \frac{M_0}{H_0}\right) + (\omega_z\tau)^2} \tag{24}$$

and

$$\hat{m}_x = \frac{M_0}{H_0} \cdot \frac{(\omega_z \tau)\,\hat{h}_y + (j\xi\tau + 1)\dfrac{\hat{b}_y}{\mu_0}}{(j\xi\tau + 1)\left(j\xi\tau + 1 + \dfrac{M_0}{H_0}\right) + (\omega_z \tau)^2} \tag{25}$$

The complex amplitudes $\hat{m}_x$ and $\hat{m}_y$ of the transversal magnetization are still undetermined quantities.

3. CONCLUSION

As it will be seen in further analysis, in the case of absence of fixed flux the spin velocity and $\hat{m}_x$ and $\hat{m}_y$ are space invariant. When the flux is fixed the spin velocity together with $\hat{m}_x$ and $\hat{m}_y$ vary with varying of the width of y. The second term in (1) contributes nothing, as to the velocity of the flux along x and at $\partial/\partial z$ magnetization is zero.

In magnetic fluids the magnetization increases in the rotating (spiral) form, as to at the rotation it itself is responsible for movement of the fluid with the spin velocity ω_z, differing from zero, which itself changes the magnetization.

Thus, just like the relaxation of magnetic fluids, the mechanical equations should be taken into account and solutions for ω_z, $\hat{m}_x$ and $\hat{m}_y$ should be received.

REFERENCES

[1] D. Giancoli, "Physics Principles with Applications", New Jersey, 1995.

[2] K.M. Koch, P.B. Brown, D. L. Rothman and R.A. de Graaf, "Sample Specific Diamagnetic and Paramagnetic Passive Shimming", US National Library of Medicine, September 2006.

[3] K. V. Kotetishvili and G. G. Chikhladze, "Linearization of Langevin's Equation in Magnetic Fluids", J. Nano-Studies, 2013.

EXPERIMENTAL INVESTIGATION ON SPACE CONFIGURATION AND INFLUENCE OF ELECTROMAGNETIC FIELD OF SHORT WAVE APPARATUSES IN MEDICAL THERAPY

D. Dimitrov and A.P. Petrova

Faculty of Telecommunications, Technical University of Sofia, Bulgaria
1000 Sofia, "Kl. Ohridsky" str.8
dcd@tu-sofia.bg

Abstract

The usage of short waves in the medical therapy started to become quite popular in the recent decades. The space-time configuration research of the electromagnetic field in the patient area within the UHF range is really important for the treatment used in physiotherapy methods. Based on the results of this study are defined the system's mode which induce the electromagnetic field in the patient area, the number of the therapeutic procedures and duration of each of them. The radiators (antennas) in the physiotherapy are often in proximity to the patient's body, i.e it is necessary to consider the impact of the body to the patient, the parameters of the antenna and to the research of the area in the near field. In this paper are presented and described in graphic form the conducted studies for electromagnetic field strength in the very near field in real clinical conditions.

At high frequencies, polarizing molecules are in the patient's body completely failed changing their spatial orientation and appear vibrations of the dipoles around neutral position. This process is related to the generation of heat. A characteristic feature of UHF waves impact on the body that the heat is produced within the body itself. In physiotherapy are used transmitters, which excited the electrical field for the induction of these frequencies. A pair of two "electrodes" usually acts as antenna system on these devices. The antenna system is ensuring the influence of the electromagnetic field of a small part of the human body.

1. INTRODUCTION

In the theory of antennas and the distribution of electromagnetic waves are defined three areas: the first area (far field) in which the angular distribution of the field is independent of the distance from the antenna and the emitted wave is spherical. The second zone is the very near radiating field (Fresnel zone) in which the angular distribution of the field depends on the distance from the antenna. In this area radiated wave, which is actually a plane wave, is gradually becoming a spherical wave. The third area is the near reactive field, which is located at a distance between

0 and λ/2π from the antenna where the reactive field dominates. It is the area of interest in medical systems for the physiotherapy. For an antenna with a maximum size, which is small compared to the wavelength, the energy in the very near field is mostly reactive. This stored energy is transmitted periodically from the antenna to the near field. The reactive near field extends from the antenna to a distance "R" from the antenna. The formula for calculation of this distance is:

$$R = \frac{\lambda}{2\pi} \tag{1}$$

where λ is the wavelength.

2. EXPERIMENTAL INVESTIGATION ON THE SPACE CONFIGURATION OF THE ELECTROMAGNETIC FIELD

For exploring the space-time configuration in the patient area in the measurements, a transmission frequency of the device is used, which is close to the used frequency, namely – 29.5 MHz with a wavelength 10.1 m approximately. In our case, the very near field extends at a distance R = 1.62 m from the antenna, considered in the formula (1).

The definition of the two components $\vec{E}$ and $\vec{H}$ of the electromagnetic field at the revelant points of the patient area is necessary for making the desired measurements. When determining the shape of the area of the space / the plane, which the simulation is performed, the main consideration is the reporting of the mutual position of the electrodes (antennas) of the system and its emplacement to the treatment area of the patient's body. A common case in physical therapy is the used of an apparatus with a pair of emitters. It can be seen the measured antenna system with the exact location of the disc nozzle in Figura 1. [1]

Figure 1. The used antenna system with disc nozzles of each of the emitters during the study of space-time configuration of the electromagnetic field

In order to facilitate and accelerate the sampling and the calculation (simplification of the algorithms based on the use of symmetry) is appropriate the space area to be approximated by a regular geometric figure. This would be allowed using the available symmetry for optimization the developed algorithms for sampling and calculation. The used geometric figure should also cover the maximum radiating surface. If we use the formal requirement of symmetry, the suitable plane figures are rectangle, square and circle. This matches with the usual forms of radiation surfaces. In the case of a circle can be selected algorithm which completes the circle of points situated in concentric circles starting from the center. In the case of a circle can be selected algorithm which completes the circle with points, situated in concentric circles, starting from the center. [2]

To facilitate the measurement and interpretation of the results was used a graphical representation of the antenna system (placement of the vibrators relative to one another) in the vertical plane (Figure 2). Formally the figure can be considered as a trapezoid, which is in accordance with the usual position of the electrodes (antennas) of Figure 1. The mid-segment of the trapezoid (Figure 2) is the axis between the centers of the antennas. It is important to know the location of the vibrators, as they can be located closer or further away, the distance should be between 2 and 10 centimeters. And depending from their size and location, can determine the distribution of the field and the change of the temperature on the patient.

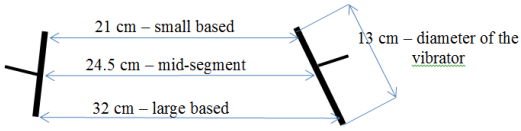

Figure 2. A graphical representation of the antenna system (position of vibrators relative to one another in the vertical plane).

3. RESULTS AND ILLUSTRATION OF THE INVESTIGATION OF THE ELECTROMAGNETIC FIELD

The measurements of the electrical intensity were made at different points in small base, large base and mid-segment on the trapezoid, and in the points of the radius of one emitter.

The measured values are in relative units, as for the electric strength and the magnetic induction. These values are related of course with the absolute values with an accuracy of one coefficient. The magnetic induction in the respective sections was calculated by the following expression:

$$\frac{E}{H} = \eta = 120\pi \approx 377\Omega \qquad (2)$$

where η is the characteristic impedance [3]

In Table 1 are given in relative units the obtained values for the electric intensity and magnetic induction in the various items of the bases and the mid-segment of the trapezoid (Figure 2) and the radius of one of the emitters in parallel placement of the measured antenna of electrical in parallel placement of the antenna in the patient area. In Table 2 are given in relative units the obtained values for the electric intensity and magnetic induction in the various items of the bases and the mid-segment of the trapezoid (Figure 2) and the radius of one of the emitters when the measured antenna measurement is perpendicular of electrical line of force.

Table 1. Relative values of the measured levels of electric intensity E and magnetic intensity H in parallel placement of the antenna in the patient area

Small base		*Mid-segment*		*Large base*		*Radius*	
E	H	E	H	E	H	E	H
77,1	0,204	64,1	0,17	77,3	0,205	75,5	0,2
77,8	0,206	67,4	0.179	78,3	0,208	74,5	0,198
77,7	0,205	65,7	0.174	77,8	0,206	72,5	0,192

Table 2. Relative values of the measured levels of electric intensity E and magnetic intensity H in perpendicular placement of the antenna in the patient area

Small base		Mid-segment		Large base		Radius	
E	H	E	H	E	H	E	H
78,1	0,2072	61,9	0,1642	77,6	0,2058	77,8	0,2064
78,5	0,2082	64,5	0,1711	78,2	0,2074	76,2	0,2021
78,2	0,2074	62,4	0,1655	78	0,2069	75,2	0,1994

In Figure 3 is illustrated a screen of the spectrum analyzer for measuring the relative level of the electrical intensity. The tick is for a broadcasting frequency, together with significant harmonic of the radiation to the right of the main tick. These harmonics appear, as the apparatus is operated in the mode of the amplitude manipulation. The amplitude manipulation is a method often used in the physiotherapy, in order to avoid the adaptation of the patient to the parameters of the influence electromagnetic field and thus to provide, if necessary, a longer course of treatment for more severe disease. The screen of the spectrum analyzer can be seen in figure 4, where is the oscillogram of the broadcasting amplitude manipulated signal.

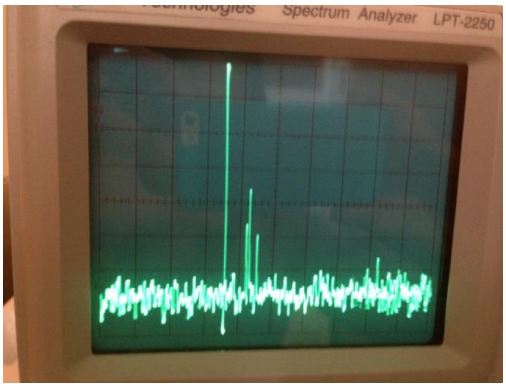

Figure 3. A screen of spectrum analyser at measurement of the relative level of electric intensity

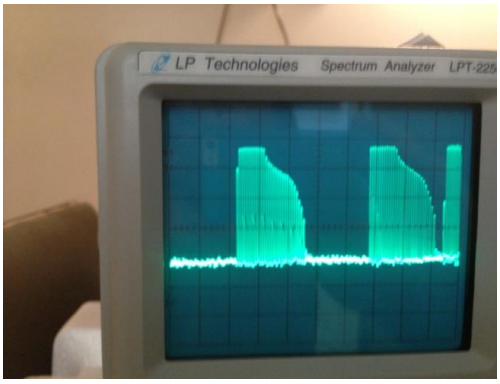

Figure 4. The oscillogram of the broadcasting amplitude manipulated signal

In graphical form are the results of the measurements are given in Table 1 and Table 2 below. The results, from the measurement of the electric intensity and the

calculated values of the magnetic induction on the three bases of the trapezoid small, large and mid-segment in parallel placement of the measured antenna and the electrical line of force in the near field, are present in Figure 5 and Figure 6. Figure 7 and Figure 8 shows the results, from the measurement of the electric intensity and the calculated values of the magnetic induction on the three bases of the trapezoid small, large and mid-segment in perpendicular placement of the measured antenna and the electrical line of force in the near field. Figure 9 and Figure 10 shows the results, from the measurement of the electric intensity and the calculated values of the magnetic induction on the three bases of the trapezoid small, large and mid-segment in parallel and perpendicular placement of the measured antenna and the electrical line of force in the near field. The functions shown in the figure from 5 to 10 were obtained as discrete values in the result of the measurements of the electrical intensity in a finite number of points. If the obtained discrete values of the functions are connect with the segment, could be regarded that the made a simple interpolation, so that they can take into account the relative values of the variables and between points of measurements. This is shown by points 1 and 2 on the charts. In mathematics certainly has quite analytical methods for interpolation, which may be used in the requirement for greater accuracy in the interpolation.

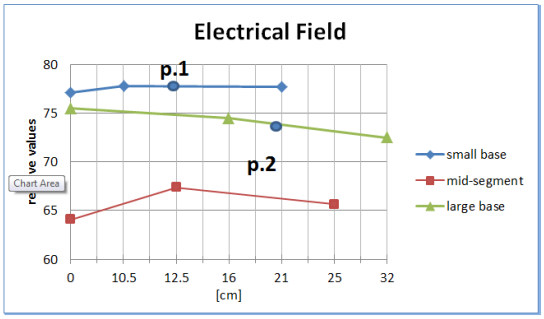

Figure 5. Relative values of the electrical intensity of the three axes: small, mid and large segment in parallel placement of the measured antenna

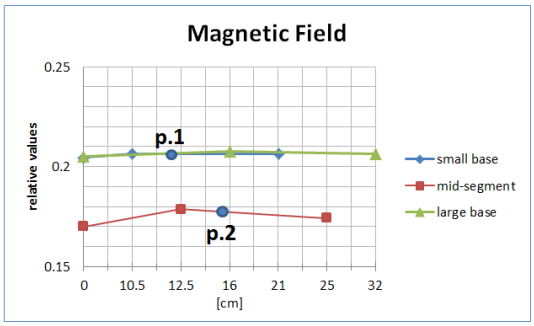

Figure 6. Relative values of the magnetic induction of the three axes: small, mid and large segment in parallel placement of the measured antenna

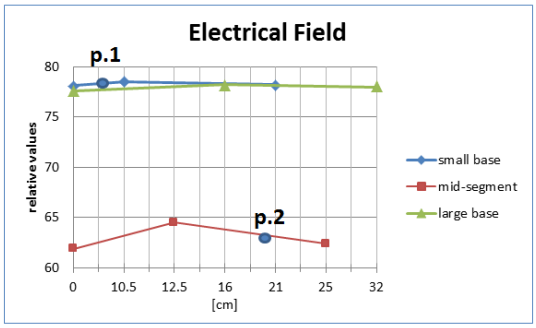

Figure 7. Relative values of the electrical intensity of the three axes: small, mid and large segment in perpendicular placement of the measured antenna

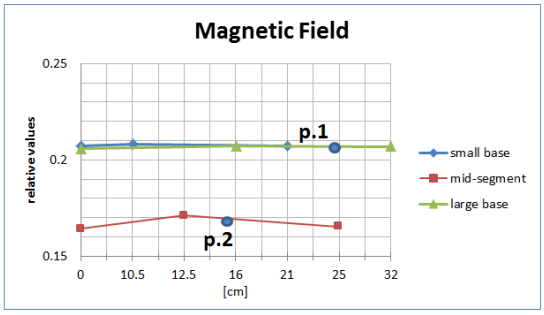

Figure 8. Relative values of the magnetic induction of the three axes: small, mid and large segment in perpendicular placement of the measured antenna

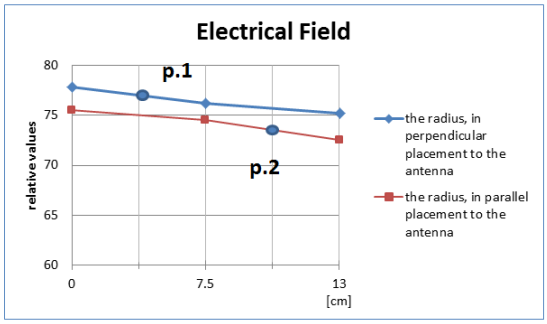

Figure 9. Relative values of the electrical intensity at the radius in parallel and perpendicular to the measured antenna

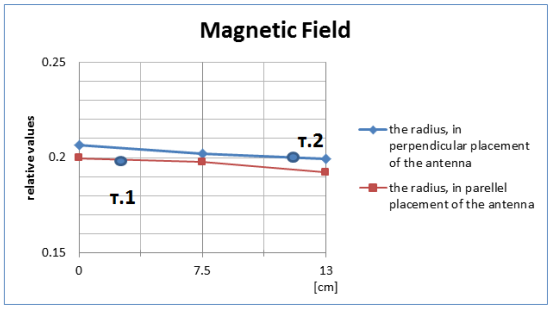

Figure 10. Relative values of the magnetic induction at the radius in parallel and perpendicular to the measured antenna

Experimental measurements of the strength of the electric field in the very near field in actual clinical conditions were made in the conventional mode, used in the course of therapy, namely, continuous transmission mode and a mode of amplitude manipulation of the electromagnetic field.

3. CONCLUSION

In conclusion we can say that the study of the characteristics of electromagnetic field in the nearby area along with the study and optimization of the space-time configuration of the electromagnetic field are very important and crucial for achieving the desired therapeutic effect. These waves have similar physiological action with the other high frequencies currents, but they penetrate to greater depths. Ultra-high frequency waves have a good therapeutic effect in: transient disorders of cerebral circulation, stroke, vascular incidents in the central nervous system, chronic arterial insufficiency of lower extremities. Improves microcirculation, rheological properties of blood, detection of shunting, increased cell permeability.

REFERENCES

[1] D.Dimitrov, "Medical systems influence of electromagnetic fields on human" ,education book, TU-Sofia,2007

[2] W.Y. Riadh, "Electromagnetic Fields and Radiation (Human Bioffects and Safety)",Marcel Dekker Inc. Canada,2001,ISBN 0-8247-0877-3

[3] S.Laybros and P.F.Combes, "On Radiating Zone Boundaries of Short, λ/2 and λ Dipoles", IEEE Antennas and Propagation Magazine,45,5,October 2004,pp. 53-64.

MEASUREMENT AND COMPARISON OF LTE AND HSPA+ NETWORK PARAMETERS

D. Rukavičius, V. Grimaila and S. Kašėta

Department of Telecommunications, Kaunas University of Technology,
Studentu st. 50, LT-51368 Kaunas, Lithuania
darius.rukavicius@gmail.com

Abstract

Long Term Evolution (LTE) network parameters are analysed in this paper. 3GPP LTE Release 8 specifies peak downlink throughput up to 100 Mbps using SISO antennas and up to 300 Mbps using 4x4 MIMO antennas. According Channel Quality Indicator (CQI) and Received Signal Strength Indicator (RSSI) indexes the Physical Downlink Shared Channel (PDSCH) download throughput of LTE network there is analysed in dependency of distance from base stations. Throughput values are compared with the results of High Speed Packet Access (HSPA+) network measurements as this is earlier technology for data transfer. HSPA+ and LTE networks measurements were made in implemented real network in real time. As LTE network on measuring time was not used by other users yet, the results of analysis can be considered as received in real and close to ideal conditions. HSPA+ network was used by users, but values are close to ideal as the network was newly implemented.

1. INTRODUCTION

LTE is the new access part of the Evolved Packet System which is only IP based. High spectral efficiency, high peak data rates, short round trip time and frequency flexibility are the main requirements for the new access network.

The LTE access network is a network formatted of base stations, evolved NodeB (eNB). There is no centralized intelligent controller, and the eNBs are normally inter-connected by the X2-interface and towards the core network by the S1-interface (Fig. 1). The reason for distributing the intelligence amongst the base-stations in LTE is to speed up the connection set-up and reduce the time required for a handover. For an end-user the connection set-up time for a real time data session is in many cases crucial, especially in on-line gaming. The time for a handover is essential for real-time services where end-users tend to end calls if the handover takes too long [1].

The CQI indexes and SNR values in signal receiving places are the main parameters that indicate LTE efficiency and quality. These indexes and values are affected by various factors. CQI and SNR are directly influenced by algorithms used

between user equipment (UE) and eNBs for data transmitting. As information in International Journal of Information and Electronics Engineering shows, SNR and CQI can be mapped and affect each other [2] and CQI index influences throughput of LTE networks [3].

Our subject of interest is the mapping distance from base station impact to the network data throughput, as no information about such measurements can be found in installed or tested LTE networks. Comparison of throughput values in HSPA+ and LTE network will also show the difference of technologies and projected user experience. Measurement results can be used in the future for planning the implementation of LTE network eNB's in cities with medium density.

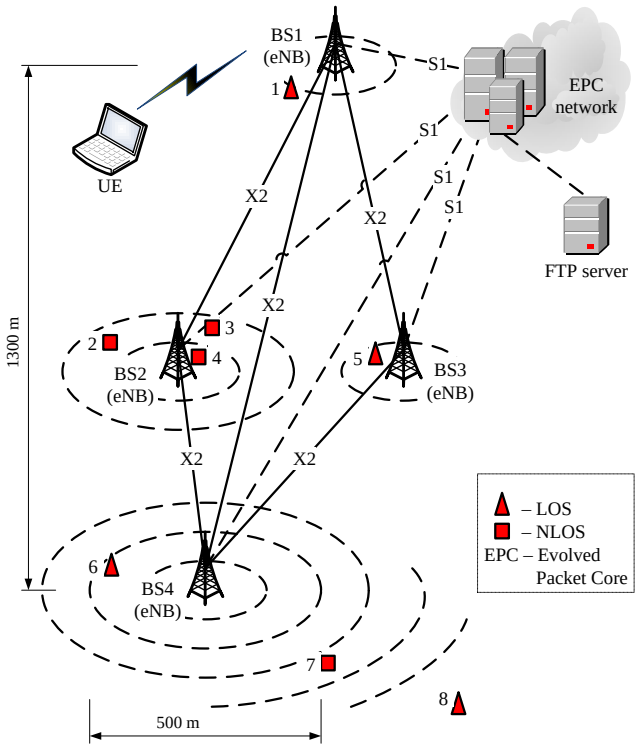

Figure 1. Deployment of LTE network base stations

2. MEASUREMENT CONDITIONS

HSPA+ and LTE network parameters were measured in medium density city center. Deployment of LTE network base stations is presented on Fig. 1. Base stations in this city are installed in 30–40 m height and buildings are with average height of 20–30 meters. LTE network is implemented by one of mobile operator. Network operates on 1800 MHz frequency on FDD mode and uses 2x2 MIMO with 20 MHz

bandwidth channel. Measurements were made using TEMS Investigation software and Huawei UE. Weather conditions were without precipitations.

HSPA+ network is implemented throughout all medium density city (the same as LTE network) with the coverage of the whole area. HSPA+ operates on 1800 MHz frequency on FDD mode and uses 1x2 SIMO with 5 MHz bandwidth channel. Measurements were made using TEMS Investigation software and Huawei UE. Weather conditions were without precipitations.

The points for LTE network measurements were taken using standard user model. As ordinary users do not choose places with better parameters, measurements were done using different conditions: distance from base stations (BS), line of sight or not, orientation to BS antenna. HSPA+ network was measured using the same model, about 100-150 m distance from base station.

LTE measurement points are divided to categories: Line of Sight (LOS) and Non Line of Sight (NLOS). This was done, as some point have clear visibility to eNB, and some do not. As the parameters of LTE network depend from this factor, more exact analysis is done using LOS and NLOS models. Measurements made for BS1, BS3 and some BS4 were in LOS conditions, and BS2 and some BS4 points satisfy NLOS conditions (see Fig.1).

3. MEASURED PARAMETERS

Measured and analyzed parameters of LTE network were: PDSCH throughput, CQI index, RSSI index, Reference Signal Received Power (RSRP) and Reference Signal Received Quality (RSRQ).

The PDSCH is the main data bearing channel which is allocated to users on a dynamic and opportunistic basis.

PDSCH is used to transfer application data. The throughput achieved by the PDSCH depends upon the [4]:

- number of resource elements allocated to the PDSCH;
- modulation scheme applied to each resource element;
- quantity of redundancy included by physical layer processing;
- use of multiple antenna transmission schemes.[4]

The measurements and feedback that relate to the transmission settings are known as CQI. Depending on that value (CQI index), the eNB takes the decision to assign a

particular MCS (modulation and coding scheme) for a particular UE. The higher CQI index (ranging from 0 up to 15) the higher the modulation and coding scheme and the higher the throughput. However it is up to the implemented receiver algorithms in the UE, at which signal to noise plus interference (SNIR) the good throughput can be achieved (the algorithms are vendor dependent so the "good SNIR" may vary for various UEs). CQI index values presented in 3GPP LTE specification are shown in Table 1.

In HSPA+ network there were measured throughput and CQI index parameters.

Channel quality indicator shows what the value of signal quality is and by this value UE decides what modulation and transport block size to use. As shown in Table 2, CQI values range is between 0 and 30.

TABLE 1. CQI VALUES IN LTE NETWORK [5]

CQI index	**Modulation**	**Code Rate x 1024**	**Efficiency**
0	No transmission	out of range	
1	QPSK	78	0.1523
2	QPSK	120	0.2344
3	QPSK	193	0.3770
4	QPSK	308	0.6016
5	QPSK	449	0.8770
6	QPSK	602	1.1758
7	16QAM	378	1.4766
8	16QAM	490	1.9141
9	16QAM	616	2.4063
10	64QAM	466	2.7305
11	64QAM	567	3.3223
12	64QAM	666	3.9023
13	64QAM	772	4.5234
14	64QAM	873	5.1152
15	64QAM	948	5.5547

TABLE 2. CQI VALUES IN HSPA+ NETWORK [6]

CQI value	Modulation	CQI value	Modulation
0	Out of range	16	16QAM
1	QPSK	17	16QAM
2	QPSK	18	16QAM
3	QPSK	19	16QAM
4	QPSK	20	16QAM
5	QPSK	21	16QAM
6	QPSK	22	16QAM
7	QPSK	23	16QAM
8	QPSK	24	16QAM
9	QPSK	25	16QAM
10	QPSK	26	64QAM
11	QPSK	27	64QAM
12	QPSK	28	64QAM
13	QPSK	29	64QAM
14	QPSK	30	64QAM
15	QPSK		

4. ANALYSIS OF PDSCH THROUGHPUT DEPENDENCY FROM DISTANCE

The downlink throughput measurements were made for 4 base stations in LTE network. Every point of measurement was picked taking different distances from base station to UE every time. As mentioned above, measurements were in LOS and NLOS conditions. Average and peak values are shown in the graphics.

Fig. 2 shows average and peak throughput dependency from eNB to UE distance in LOS conditions. As it can be seen, even if the throughput maximum values vary in wide range for BS1 (up to 184 Mbps) and BS3 (up to 120 Mbps), the measured average throughputs are similar (respectively 52.2 Mbps on point 1 (see Fig.1) and 52.6 Mbps on point 5). For BS4, distance from eNB to UE is higher (point 8), so measured peak throughput is lower (24.6 Mbps). Measured peak throughput (33.8 Mbps) on point 6 could be higher, but measurement was done on the edge of cell coverage, so it was influenced by adjacent cells interferences. Measurement results indicate an average throughput decreasing tendency when distance from eNB to UE is increased.

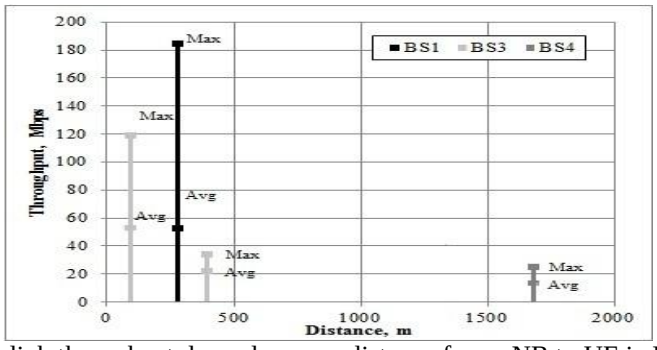

Figure 2. Downlink throughput dependency on distance from eNB to UE in LOS conditions

Fig. 3 shows average and peak downlink throughput dependency from distance in NLOS conditions. The throughput maximum values vary in wide range for BS2 (up to 47 Mbps on point 4, up to 44 Mbps on point 3 and up to 38 Mbps on point 2) and for BS4 (up to 43 Mbps on point 7), and the measured average throughputs are similar in these points (respectively 22 Mbps on point 4, 21 Mbps on point 3, 23 Mbps on point 2 and 26 Mbps on point 7). We suppose there was no throughput decreasing tendency because there were less and lower buildings near BS4.

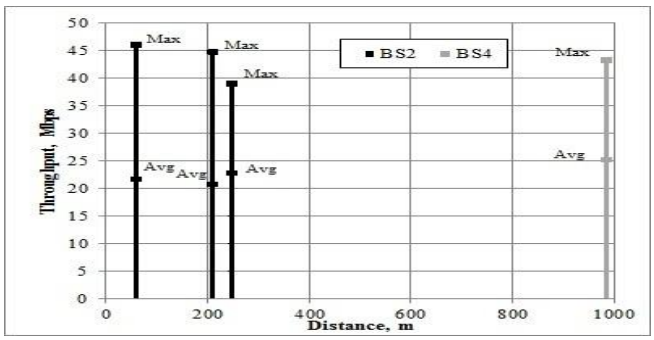

Figure 3. Downlink throughput dependency on distance from eNB to UE in NLOS conditions

5. ANALYSIS AND COMPARISON OF THROUGHPUT VARIATION DURING FILE TRANSMISSION PROCESS

In Fig. 4, Fig. 5 and Fig.6 are presented results of the throughput variation during file transmission processes in LTE network, respectively on point 1 (LOS) and point 2 (NLOS) and HSPA+ network.

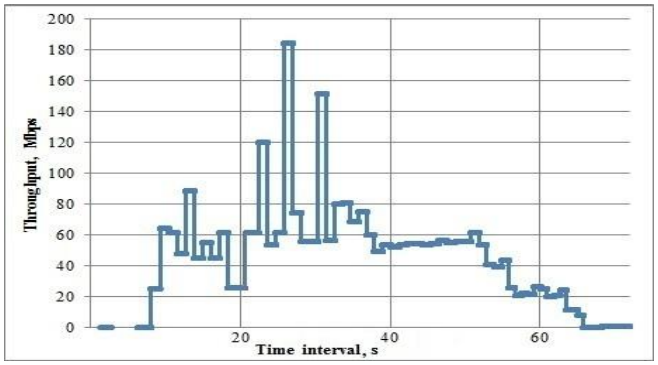

Figure 4. Downlink throughput during transmission process in LOS

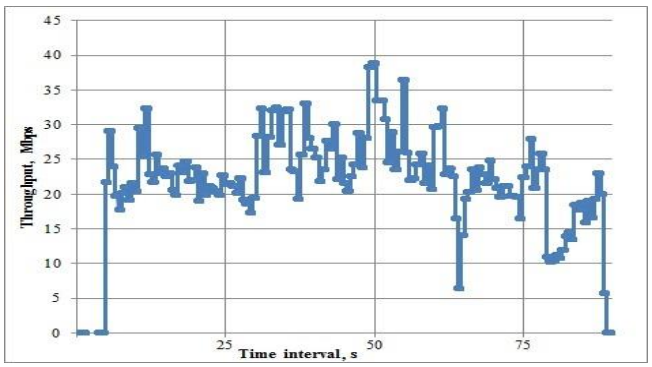

Figure 5. Downlink throughput during transmission process in NLOS

As can be seen from Fig.4, the downlink throughput values initially vary by more than 9 times. In the middle of the process the throughput variation is practically constant, and decreases by the end of file transfer.

As can be seen from Fig. 5, the downlink throughputs changes throughout the transmission process varying by more than 6 times, and file transmission process elongate.

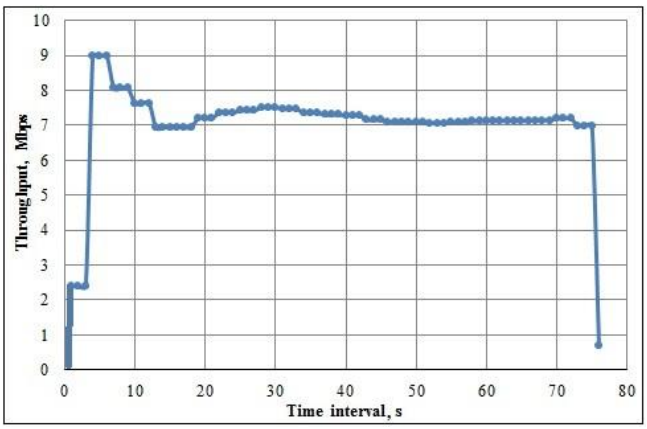

Figure 6. Downlink throughput during transmission process in HSPA+ network

As can be seen from Fig.6, throughput is not varying so much as in LTE network (LOS and NLOS conditions) and the value changes up to 20 %. The values differ

from LTE network up to 20 times in LOS conditions and up to 4 times in NLOS conditions.

6. ANALYSIS OF PEAK THROUGHPUT DEPENDENCY FROM CQI

As was mentioned before, CQI indicator shows what modulation and what effectiveness are in the network. Therefore, the higher CQI, the higher peak throughputs can be measured.

In Fig. 7 are presented results of peak throughputs on eNB's and corresponding CQI indicator values given by the network in LOS conditions. On point 1 (BS1) peak throughput was 184 Mbps, which was measured when CQI value was 14. At this indicator value 64QAM modulation is used, and high throughputs can be achieved. On point 5 (BS3) CQI indicator value was 11, and throughput was 120 Mbps. So there can be done conclusion, that when CQI indicator values are between 11 and 15, i.e. 64QAM modulations are used, the throughputs higher than 100 Mbps can be achieved.

On far off point 8 (BS4) CQI indicator value was 8, 16QAM modulation was used, and peak throughput was only 24 Mbps. On point 6 (BS4) CQI indicator value was 14, but achieved throughput was only 38 Mbps.

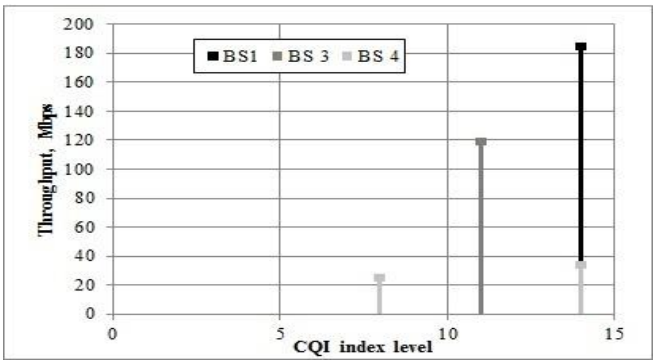

Figure 7. Downlink peak throughput dependency from CQI in LOS

As we can see from Fig. 8, in NLOS conditions, the throughput values are by comparison low (between 38 Mbps and 47 Mbps on points 2, 3, 4 and 7) independently what CQI indicator values are (between 8 and 15), i.e. independently what modulation 16QAM or 64QAM is used. Also we can see, that on point 4 (BS2) CQI indicator value is only 8, but downlink throughput, that was achieved, is maximum in this group.

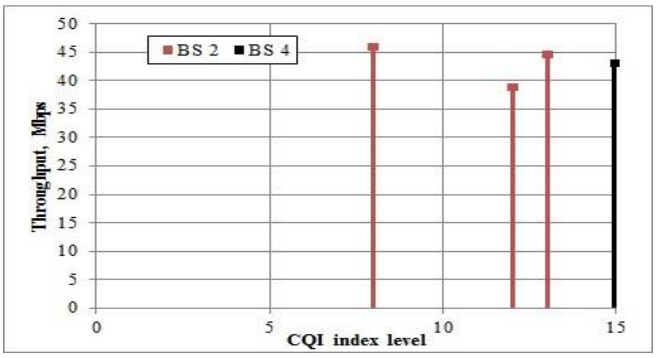

Figure 8. Downlink peak throughput dependency from CQI in NLOS

Therefore, no matter in LOS or in NLOS conditions, CQI indicator is not enough for specify the quality of network and more deep investigations are required for this problem.

As mentioned above, in HSPA+ network CQI values are from 0 to 30, which are differing from LTE network. In Fig. 9 it can be seen, that there is a direct correlation between CQI index level and measured throughput. But there can be seen that difference in throughputs are almost the same, when CQI value is 25 and 26, when used modulation is 16QAM (when CQI index is 25) and 64QAM (when CQI index is 26). Even if all the points, where measurements were made, are in similar conditions, throughput values differ and can be low as 3 Mbps by CQI value of 27. That means that not only CQI values influence throughputs.

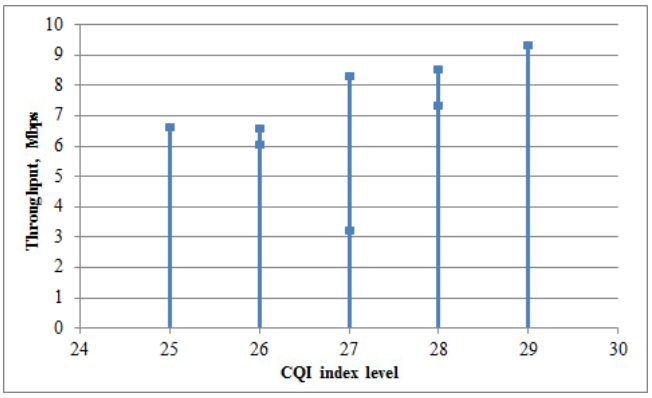

Figure 9. Downlink peak throughput dependency from CQI

7. ANALYSIS OF CQI DEPENDENCY FROM DISTANCE

During implemented LTE network measurements was observed CQI indicator values dependency on the distance from eNBs to UE.

As it can be seen from Fig. 10, average CQI indicator value vary from 11 to 15, when distance from eNB to UE in LOS conditions vary in range from 95 to 1600

meters. These results show that UE being close to BS, network quality parameters cannot be achieved very high. Furthermore, with increasing distance from eNB up to 1600 m, average CQI indicator value decreases only to 13.

The highest CQI indicator value 15 was obtained on point 1 (BS1), when distance from base station was 280 meters.

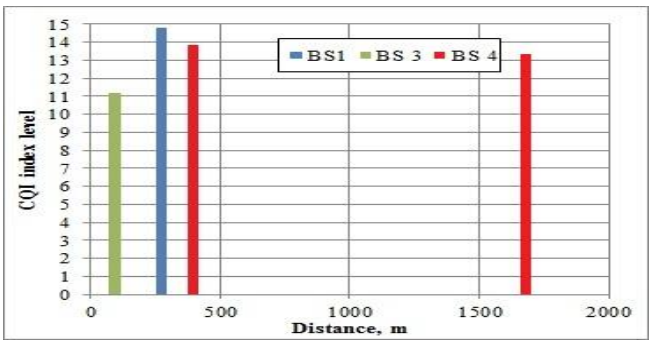

Figure 10. CQI level dependency on distance from eNB to UE in LOS

As it can be seen from Fig. 11, in NLOS conditions, we can find in near distances similar but lower as in LOS conditions CQI indicator values. There we can make assumptions: 1) no matter in LOS or in NLOS conditions, in very close distances to BS low CQI values can be influenced due to antenna declination angles; 2) highest CQI value on far point 7 (990 m from eNB) can occur as a result of multipath effect.

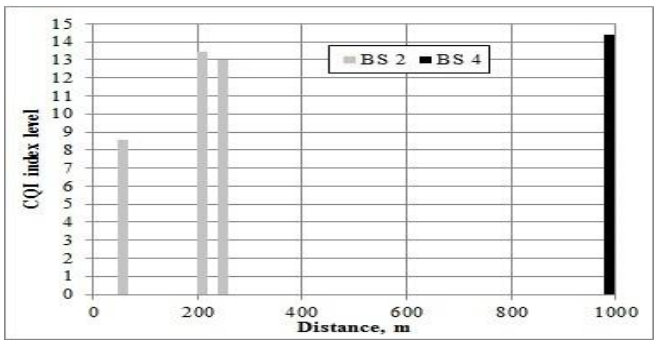

Figure 11. CQI level dependency on distance from eNB to UE in NLOS

8. CONCLUSIONS

1. No matter in LOS or in NLOS conditions, the distance from eNB to UE directly influences PDSCH throughput and other LTE network parameters such as CQI, RSSI and RSRP values.

2. In close distance (up to 280 m) from eNB to UE (in chosen cells of city) highest peak downlink throughput values (up to 184 Mbps) were measured in LOS

conditions. In NLOS conditions highest peak downlink throughputs was only up to 47 Mbps.

3. In HSPA+ network where measurements are made in close distance (100-150 m) from eNB to UE, peak throughputs are up to 9.28 Mbps and these values are up to 20 times less than in LTE network (LOS conditions).

4. During typical file transmission process in LOS conditions the downlink throughput values variation is more than 9 times. In NLOS conditions the downlink throughput variation decreases (more than 6 times) and equalizes but transmission process elongate up to 50 %.

5. In HSPA+ network, file transmission process is stable, and throughput values changes up to 22 % in the first 15 s of the process, and then it differs up to 5 %.

6. No matter in LOS or in NLOS conditions, varying distance from eNB to UE from 60 m to 1600 m CQI values stay up on high level, although CQI indicator is not enough for specify the quality of LTE network.

REFERENCES

[1] 3GPP LTE overview, [Online]. Available: http://www.3gpp.org/LTE

[2] Mohammad T. Kawser, Nafiz Imtiaz Bin Hamid, Md. Nayeemul Hasan, M. Shah Alam, and M. Musfiqur Rahman, “Downlink SNR to CQI Mapping for Different Multiple Antenna Techniques in LTE“. International Journal of Information and Electronics Engineering, Vol. 2, No. 5, September 2012.

[3] Stefan Schwarz, Christian Mehlfuhrer and Markus Rupp, “Low Complexity Approximate Maximum Throughput Scheduling for LTE”. [Online]. Available: http://publik.tuwien.ac.at/files/PubDat_187402.pdf

[4] Chris Johnson, “Long Term Evolution IN BULLETS”, 2nd Edition.

[5] 3GPP, “Technical Specification Group Radio Access Network; Evolved Universal Terrestrial Radio Access (E-UTRA); Physical layer procedures Release 11”, September 2012. [Online]. Available: http://www.3gpp.org/ftp/Specs/html-info/36213.htm

[6] 3GPP “Technical Specification Group Radio Access Network; Physical layer procedures (FDD), Release 8”, September 2009. [Online]. Available: www.3gpp.org/ftp/Specs/html-info/25214.htm

RF EXPOSURE SIMULATION USING BLOOD PERFUSION FOR A CHILD AND WOMAN MODELS

V. Jeladze, M. Prishvin and R. Zaridze

Tbilisi State University, Laboratory of Applied Electrodynamics and Radio Engineering
3, Chavchavadze Ave. Tbilisi, Georgia
veriko.jeladze001@ens.tsu.edu.ge

Abstract

It is known, that conventional Pennes bio-heat equation does not consider blood perfusion. The motivation of this paper is to conduct a comparative analysis of the temperature and temperature rise during EM exposure, obtained using conventional pennes bio-heat equation and a modified model considering blood perfusion. The non-homogeneous discreet models of a child and a woman were used for simulation.

1. INTRODUCTION

The bio-heat equation [1] has been used for many years to simulate heat exchange in human tissues. This equation does not account heat transfer effects by the blood. Several independent methodologies to overcome this limitation have been developed [2-4]. The authors of this article proposed their own approach to the problem [4]. The modified bio-heat equation presented in [4] has been used to calculate temperature and temperature rise. For the numerical calculations a child and a woman voxel models from virtual family [5] were used. The simulation has been conducted at 300MHz, 1900MHz and 3700MHz frequencies using a dipole antenna located at 10mm distance from the head model. These frequencies have been selected due their use in everyday life, 300MHz for radio communications, 1900MHz for GSM networks and 3700MHz for other wireless communications and future basebands. The result of previous studies [6] has shown us the dipole antenna gives us a good qualitative approximation of a mobile handset.

2. MODELS AND METHODS

The simulations were conducted using the FDTD method. Temperature increase in tissue was simulated due to RF exposure from dipole antenna placed at 10mm distance from the head model. The EM and thermal solver FDTDLab, developed at

TSU [6, 7] was used. As it is shown in [4] the thermal solver is tested against an analytical solution for a simplified case. A sinusoidal wave signal has been used at corresponding frequency. At lower frequencies 20 dB convergence criterion was used, while at high frequencies it was 40 dB. Thus, the resultant peak temperature rises corresponded to the infinite time exposure. These factors altogether gave us an idealized model which allowed us to study the worse (with highest expected temperature rise) possible exposure scenario that can never actually take place in the real life. The frequency dependent tissue parameters for the EM simulation have been acquired from [8] and thermal tissue parameters from the virtual model have been used[5]. While it is known that there are two kinds of effects caused by the RF field: biological and thermal, only the thermal effects have been considered in this paper.

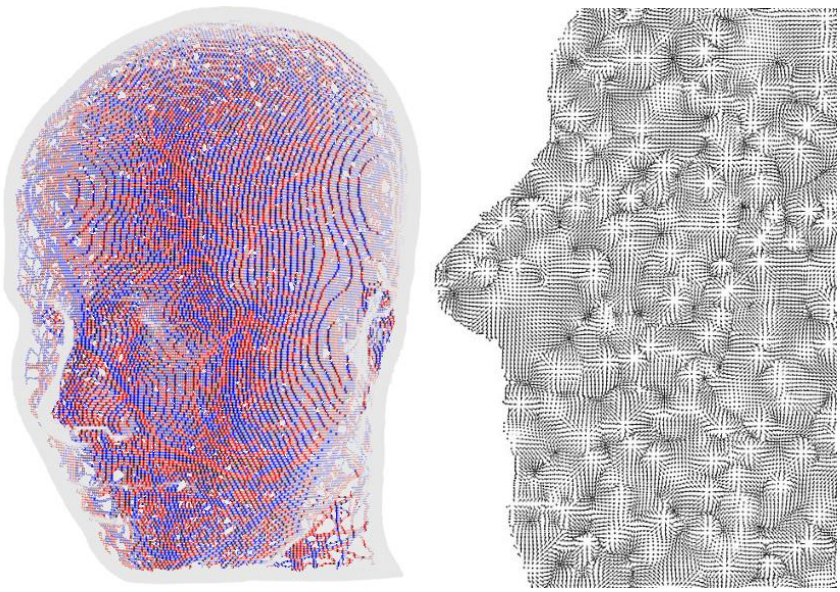

a) b)

Figure 1.a) arterial and venous vascular network in a human brain model, b) capillary blood flow in a uniform model.

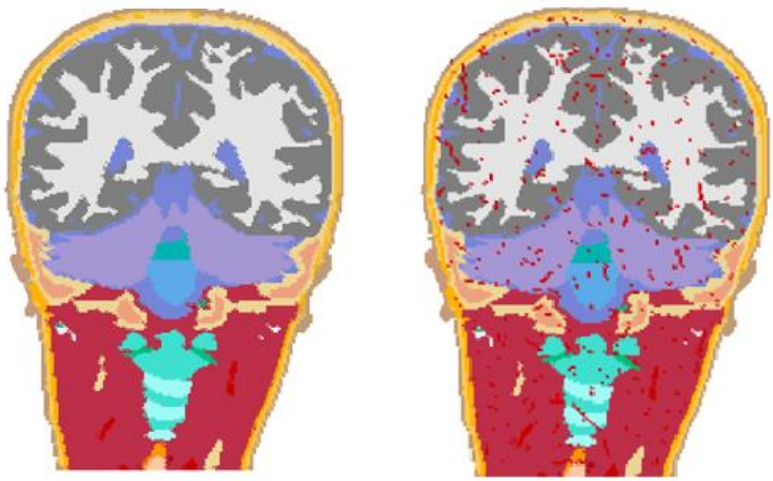

Figure 2. The voxel model with the artery and vein vessels added.

In order to use the modified bio heat equation described in [4] we have to prepare the model for simulations. It involves building the arterial and venous vascular networks (Fig.1) and calculating the capillary flow blood filed. The procedure can handle only selected tissues or the whole model. For the calculation presented in this article the model was supposed to be uniform. That means that only the enclosing geometry (like liver or lungs) was used to build the vascular network. The ear of the models has been smoothed in order to obtain more reliable EM simulation results.

As an example the vascular (in volume) and capillary networks (in one cross section) constructed for lungs are presented on Fig.3.

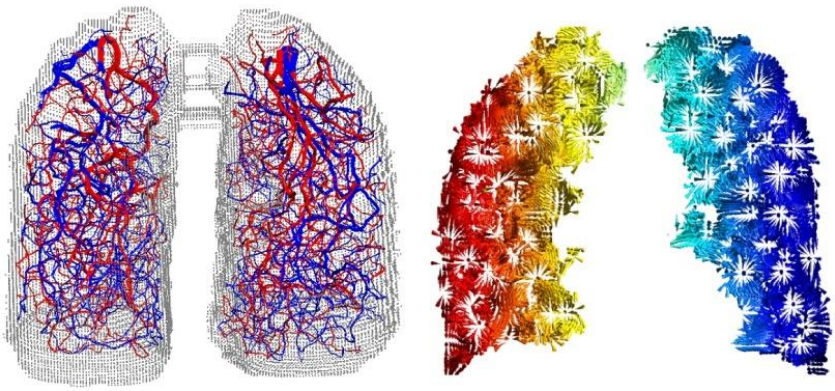

Figure 3. Vascular network and blood flow velocity vectors calculated for human lung model.

3. RESULTS OF CALCULATIONS.

The numeric results of calculations of the conventional pennes model and the modified model, correspondingly, are presented in Fig.4, Fig.5. It can be seen that the results for the conventional pennes model and the modified model [4] are in good agreement.

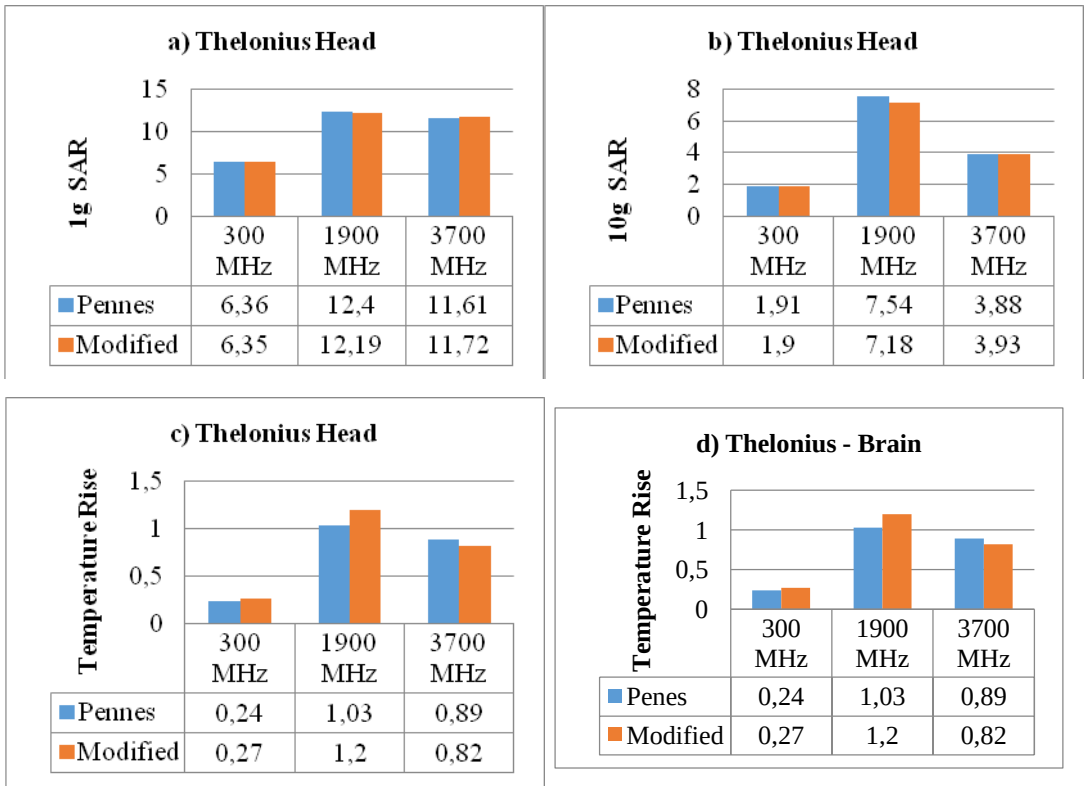

Figure 4. 1g SAR, 10g SAR and temperature rise for the Thelonius head models and temperature rise for the Thelonius brain at 300MHz, 1900MHz and 3700MHz.

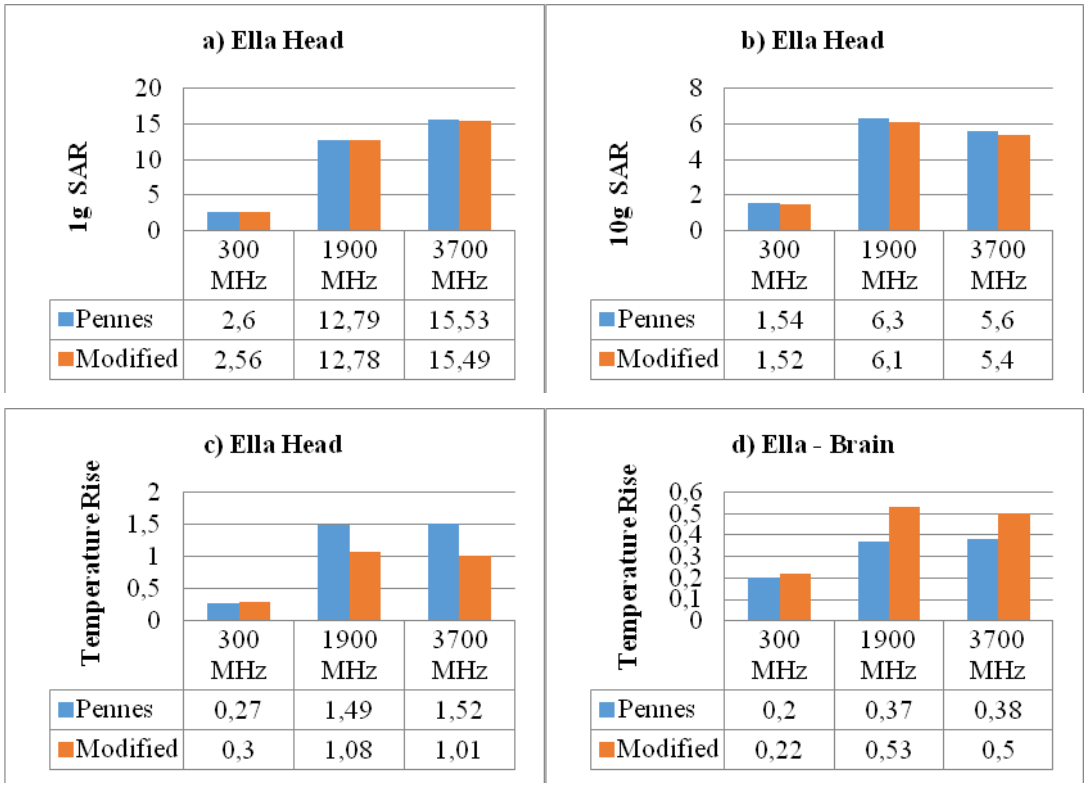

Figure 5. 1g SAR, 10g SAR and temperature rise for the Ella head models and temperature rise for the Ella brain at 300MHz, 1900MHz and 3700MHz.

The woman model is name "Ella", the child model is named "Thelonius" Fig.4, Fig.5. As we see (Fig.5c) the peak temperature rise values for the modified bio-heat equation in some cases are lower. This fact is easily explained by the smoothing of a local temperature rise. In some cases, e.g. Thelonius model at 300 MHz and1900 MHz (Fig.4c) the temperature rise for modified model is higher. It shows us that the resultant temperature rise depends on its special position and on the position of blood sources and sinks. If the temperature rise is localized near a sink the blood temperature there will higher, thus the blood will take less heat from that region. It can be also seen (Fig.4d, Fig.5d) that the peak temperature rise values in the brain are mostly higher for the modified model. At the same time for both models the peak temperature rise values in brain are smaller compared to those at the surface. These facts are explained by absorption of the EM field by outer layers and by the higher average T*b* temperature for the modified model, responsible for cooling of the tissues. It should be noted that the difference between the two models might be within the margin of error. The 1g and 10g SAR values are also close for the altered and original models. Visually the calculated distributions of the SAR values are identical Fig.6.

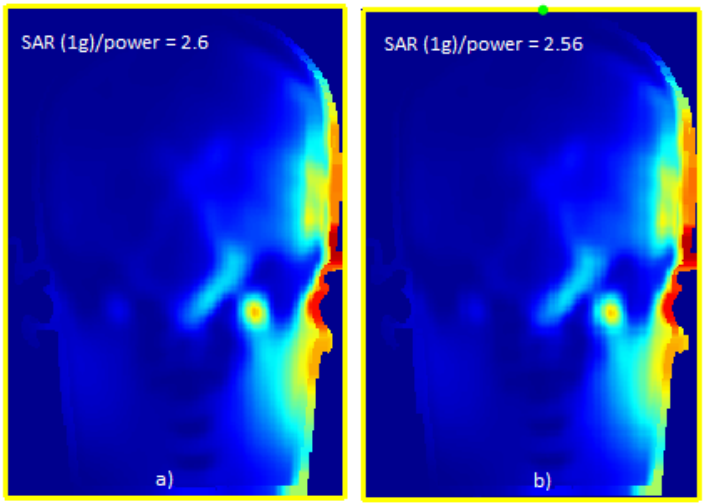

Figure 6. 1g SAR for Ella head at 300 MHz, a) pennes model, b) modified model

The calculated at 300 MHz temperature rise distributions are presented in Fig.7 (a, b) for the Pennes and the modified model respectively. It can be seen that the temperature rise distribution for the modified bio-heat equation is smoothed, and the resultant peak temperature rise is lower because of the heat diffusion. The steady state

temperature distribution is presented on Fig.8. The resultant peak temperature for the modified model is higher by about 1^0C, the temperature in all inner layers is also higher, and this corresponds to analogical results in [9]. This fact is easily explained by the higher average T_b blood temperature within the examined volume. The less is the difference between the blood temperature and the cell temperature for the given volume the less will the heat exchange between those to be. According to the obtained result the peak values of SAR and temperature rise are higher for the Ella (woman) model than for the Thelonius (child model). For both models the peak values of SAR and temperature rise are lower for low frequencies and higher for higher frequencies. This is explained by the penetration depth, which is higher at lower frequencies and the energy is distributed in a larger volume, while at high frequencies it's mostly absorbed in the thin boundary layer.

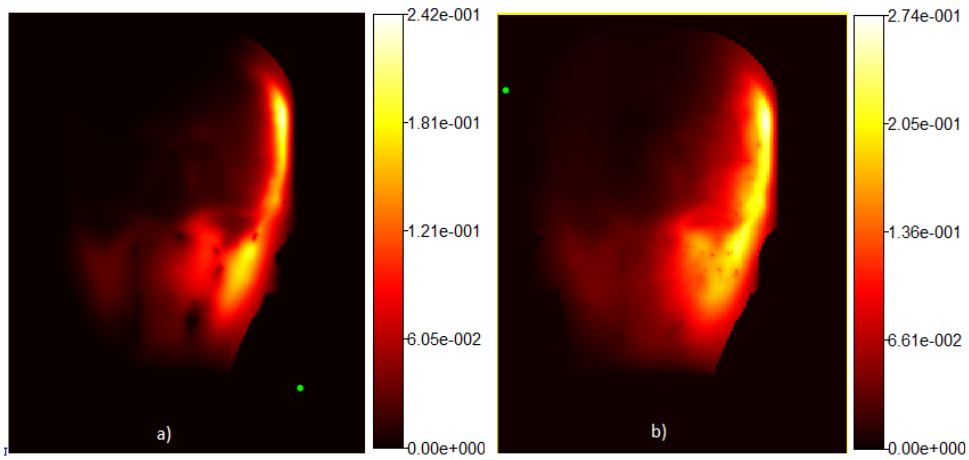

Figure 7. Temperature Rise for Thelonius head at 300 MHz, a) Pennes Model, b) Modified Model

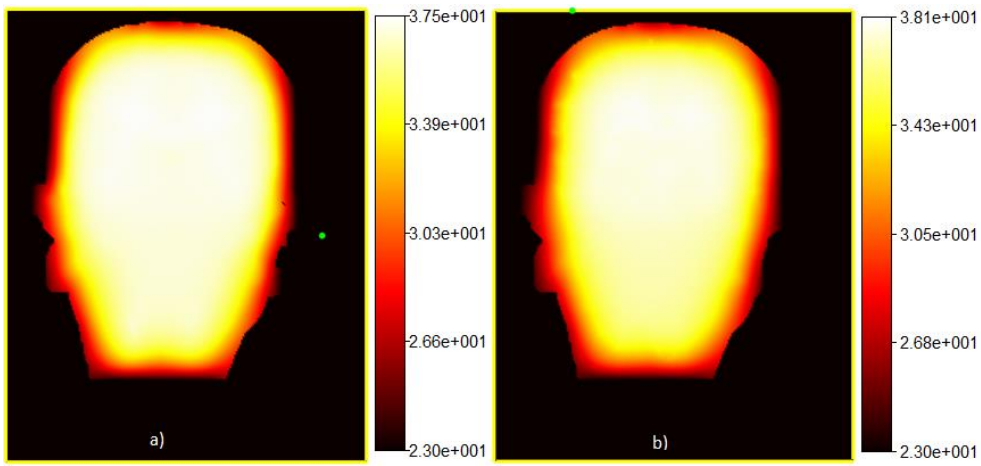

Figure 8. Temperature for Thelonius head at 300 MHz, a) Pennes Model, b) Modified Model

4. CONCLUSION

Several exposure scenarios for the modified bio-heat equation have been studied. It has been shown that the SAR and the temperature rise values for the modified model are very close to the convention Pennes equation. In most cases, when the smoothing effect played significant role the resultant temperature rise appeared to be slightly smaller. The SAR values for the modified and the original models are also in good agreement. The peak temperature, SAR and temperature rise values are lower for low frequencies and higher for high frequencies, though the peak values in the brain tissues are significantly lower compared to those at the surface for all cases. The further development of the methodology for simulation of full body exposure is planned.

ACKNOWLEDGMENT

This study is supported by Shota Rustaveli National Science Foundation grant No.30/09.

REFERENCES

[1] H. H. Pennes, Journal of Applied Physiology, vol. 1, pp. 93-102, 1948

[2]Kotte A, Van Leeuwen G, De Bree J, Van der Koijk J, Crezee H and Lagendijk J A description of discrete vessel segments in thermal modeling of tissues Phys. Med. Biol. 41, 1996,865–84.

[3]Bernardi P, Cavagnaro M, Pisa S and Piuzzi E 2003 Specific absorption rate and temperature elevation in a subject exposed in the far-field of radio-frequency sources operating in the 10–900-MHz range IEEE Trans. Biomed.Eng. 50 295–304

[4]M. Prishvin, R. Zaridze, G. Bit-Babik, A. Faraone. "Improved Numerical Modeling of Heat Transfer in Human Tissue exposed to RF energy",scientific paper, Australasian College of Physical Scientists and Engineers in Medicine, November, 2010, DOI 10.1007/s13246-010-0041-5

[5]N. Kuster. IT'IS Foundation. http://www.itis.ethz.ch/

[6]M. Prishvin, L. Bibilashvili, R. Zaridze, "Developing a thermal exemptions rationale for low-power transmitters". Journal of Applied Electromagnetism, volume 13, number 1, June 2011, pp. 39-57, http://jae.ece.ntua.gr/current.htm.

[7]M. Prishvin, L. Bibilashvili, V. Tabatadze, R. Zaridze, “Supplementary analysis of RF exposure simulations of low-power transmitters”.Journal of Applied Electromagnetism,Volume 13, number 1,June2011,pp.58-69.

[8] http://niremf.ifac.cnr.it/tissprop/htmlclie/htmlclie.htm

[9] Van Leeuwen GM, Lagendijk JJ, Van Leersum BJ, Zwamborn AP, Hornsleth SN, Kotte AN, ”Calculation of change in brain temperatures due to exposure to a mobile phone VIEW” Phys. Med. Biol. 44(10):2367-2379, 1999.